Supporting information

Tailoring D-π-A architectures with hybridized local and charge transfer fluorophore exhibiting high electroluminescence exciton utilization and low threshold amplified spontaneous emission

Lin Ma [#a], Yue Yu [#*a], Daokun Zhong [c], Chunrong Zhu [b], Xiaolong Yang [c], Zhao Feng [c], Guijiang Zhou [*c], Zhaoxin Wu [*b]

[a] School of Physics, Xidian University, Xi'an 710071, PR China.
[b] Key Laboratory of Photonics Technology for Information, School of Electronic and Information Engineering, Xi'an Jiaotong University, Xi'an 710049, PR China.
[c] School of Chemistry, MOE Key Laboratory for Nonequilibrium Synthesis and Modulation of Condensed Matter, State Key Laboratory for Mechanical Behavior of Materials, Xi'an Jiaotong University, Xi'an 710049, PR China

[*] Corresponding author: yyu@xidian.edu.cn, zhougj@mail.xjtu.edu.cn, zhaoxinwu@mail.xjtu.edu.cn

[#] These authors contributed equally to this work

Table of Contents

1. Experimental section and theoretical methodology

***General*:** The manipulation involving air-sensitive reagents was performed under an inert atmosphere of dry nitrogen. All the chemicals purchased were used without further purification unless otherwise stated. Photoluminescence (PL) and absorption spectra were recorded by a Horiba Jobin Yvon Fluoromax-4 spectrophotometer and a Hitachi UV 3010 spectrophotometer, respectively. The absolute PL quantum yields of films were measured using an integrating sphere excited at 379 nm with an absolute PL quantum yield measurement system (Hamamatsu C11347). The ^{1}H and ^{13}C NMR data were recorded on a Bruker ASCEND 500 spectrometer at 500 MHz, using tetramethylsilane (TMS) as the internal standard, $CDCl_3$ or DMSO-d_6 as solvent. Thermal gravimetric analysis (TGA) was measured on a Perkin-Elmer thermal analysis system from 50 °C to 500 °C at a heating rate of 10 °C/min under nitrogen flow rate of 80 mL/min. Differential scanning calorimetry (DSC) was performed on a NETZSCH (DSC-204) unit from 35 °C to 250 °C at a heating rate of 10 °C/min under nitrogen atmosphere. The electrochemical properties were carried out via cyclic voltammetry (CV) measurements by using a standard one-compartment, three-electrode electrochemical cell given by a BAS 100B/W electrochemical analyzer. Tetrabutylammoniumhexafluorophosphate ($TBAPF_6$) in anhydrous acetonitrile (CH_3CN) (0.1 M) were used as the electrolyte for negative or positive scan. A glass-carbon disk electrode was used as the working electrode, a Pt wire as the counter electrode, Ag/Ag+ as the reference electrode together with ferrocene as the internal standard at the scan rate of 100 mV/s. Ag/Ag+ reference electrode is commercially

available and is constituted of (1) a silver wire; (2) $AgNO_3$ solution (0.01 M) in which the $AgNO_3$ is solute and acetonitrile is solvent and (3) tetrabutylammoniumhexafluorophosphate ($TBAPF_6$) (0.1 M) which is used as supporting electrolyte.

***Devices fabrication and testing*:** The thin film doped with polystyrene (PS) in a certain amount (10 wt%) of SBz-1, SBz-2 and SBz-3 were spin-coated onto quartz substrates. ASE measurements (10 wt% doped films) were carried out for thin film samples photopumped at normal incidence with a pulsed Nd:YAG laser (5.55 ns, 10 Hz) (Surelite I, Continuum Corp, USA), using the third harmonic (355 nm). PL transient decays were measured for 150 nm thickness doped films of three compounds excitation at 360 nm. The pump stripe was perpendicular to the surface of the samples and the emitted light was collected with Fiber Optic Spectrometer (Ocean Optics SpectraSuite, USB2000). OLEDs were fabricated by thermal evaporation onto a cleaned glass substrate pre-coated with transparent and conductive indium tin oxide (ITO). Prior to organic layer deposition, ITO substrates were exposed to a UV-ozone flux for 10 min, following degreasing in acetone and isopropyl alcohol (IPA). All of the organic materials were purified by temperature-gradient sublimation in a vacuum. The devices were fabricated by conventional vacuum deposition of the organic layers, LiF and Al cathode onto an ITO-coated glass substrate under a base pressure lower than 1×10^{-3} Pa. The thickness of each layer was determined by a quartz thickness monitor. The current density-voltage-luminance (J-V-L) characteristics of devices

were measured with a Keithley 2602 and Source Meter. All measurements were carried out at room temperature under ambient conditions.

***Computational Details*:** The molecular equilibrium geometries of SBz-1, SBz-2 and SBz-3 in the S_0 states were optimized at the density functional theory (DFT) level using the CAM-B3LYP functional with the 6-311G basis set. We used time-dependent density functional theory (TD-DFT) for the calculation of the high-lying singlets and triplets excited-states with the ωB97X functional and the 6-311G basis set. The oscillator strengths and vertical excitation energy were obtained with TD-DFT based on the S_1 optimized geometry. Here, we mainly focused on the radiative decay processes, thus, based on the molecules in the S_0 optimized geometries, the vibrational frequency (ω_j) for each normal mode were calculated using the DUSHIN program developed by Weber, Cai, and Reimers [1]. Then, the Huang-Rhys factors (*S*) were calculated depending on the geometric change between the S_0 state and S_1 state and the formula are given in the Supporting Information. All the calculations were performed using the Gaussian 09 D01 program package. We further used the Multiwfn software 3.3.9 version to calculate the transition density matrix using the S_1 optimized geometry and analyze the charge-transfer process. The spin-orbit couplings (SOC) constants were estimated by the Dalton 2013 package [2].

2. Synthesis and Characterization

***Materials*:** The specific synthesis routes of these D-π-A compounds are outlined in Scheme S1, and the specific synthesis steps of these D-π-A emitters are shown below.

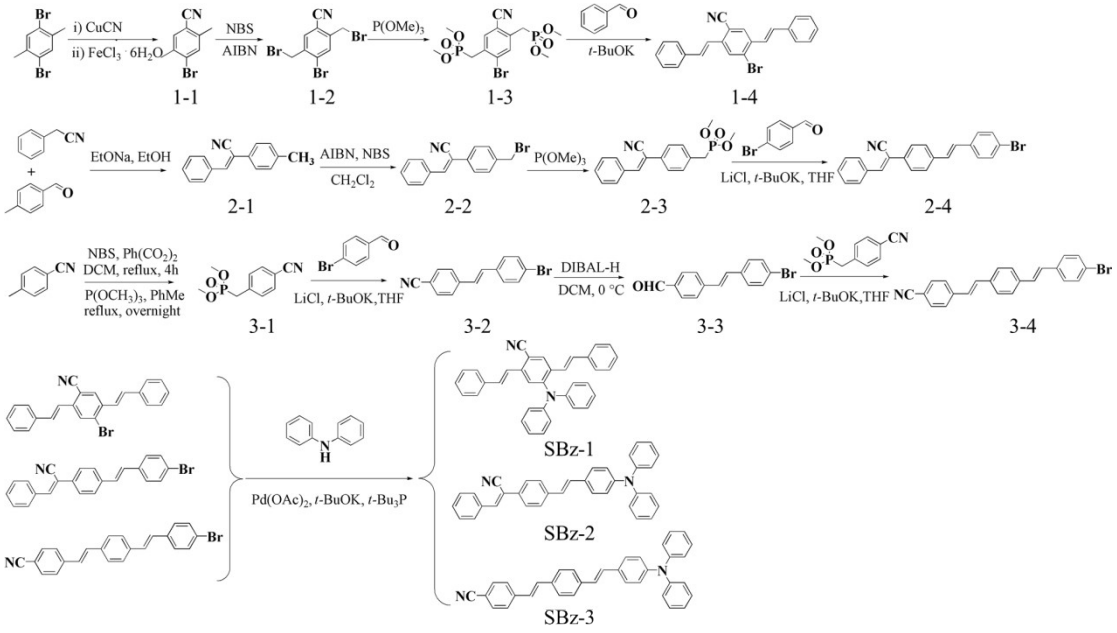

Scheme 1 Molecular structures and the synthetic routes of SBz-1, SBz-2, and SBz-3.

General Horner-Wadsworth-Emmons procedure: The phosphonic acid diethyl ester (1 equiv.) and the aldehyde (2 equiv.) were dissolved in THF and purged with Ar for 15 min. KOtBu (4 equiv.) was then added and the reaction mixture was refluxed for 30 min. under Ar atmosphere. After cooling to room temperature, the reaction was quenched with 2 M hydrochloric acid. The organic phase was isolated from the quenched reaction mixture, dried ($MgSO_4$) and evaporated to dryness. The residue was purified by chromatography on silica gel to yield the target product.

Synthesis of compound 1-1: Add Cu(I)CN (12 mmol, 1.075 g) and 1,4-dibromo-2,5-dimethyl benzene (10 mmol, 2.64 g) into DMF (50 ml). The reaction was heated to 155 °C and stirred for 16 h at this temperature. After cooling to room temperature,

a solution of $FeCl_3$ (7.9 g $FeCl_3$ in 2.5 ml concentrated HCl and 9.8 ml water) was added. The reaction was re-heated to 70 °C and stirred for 20 minutes. The mixture was allowed to cool to room temperature and then extracted with EtOAc (3 x 50 ml). The combined organic layers were washed with water (30 ml) and then brine (30 ml), dried over $MgSO_4$ and filtered. Removal of the solvent in vacuo gave a black oil which was purified by flash column chromatography on silica gel (eluting with 0% to 20% ethyl acetate in hexane gradient over 45 min. The desired product 1-1 as a purple oil, yield 650 mg, 31%. ^{1}H NMR (400 MHz, $CDCl_3$) δ: 7.50 (s, 1H), 7.42 (s, 1H), 2.48 (s, 3H) and 2.38 (s, 3H).

Synthesis of compound 1-2: compound 1-1 (2.09 g, 10 mmol), azoisobutyronitrile (AIBN) (0.16 g, 1 mmol) were dissolved in 60 mL carbon tetrachloride. N-bromosuccinimide (NBS) (5.32 g, 30 mmol) was added to the solution in batches. The mixture was stirred at 60 °C for 8 h. After cooling, the resulting mixture was poured into the ice water and filtered. The filter cake was recrystallized from petroleum ether to give 1-2 as white needle crystals, yield 2.68 g, 73.2%. ^{1}H NMR (400 MHz, $CDCl_3$, ppm) δ: 7.82 (s, 1H), 7.75 (s, 1H), 4.58 (d, J = 3.6 Hz, 4H).

Synthesis of Compound 1-3: Compound 1-2 (5.36 g, 14.7 mmol) and triethylphosphite (12.2 g, 73.5 mmol) were heated up to 90 °C for 3 h under nitrogen atmosphere. After completion, reaction mixture was vacuum distilled to remove excess triethylphosphite. Residue was triturated with pentane (10 ml) to give compound 1-3 as white solid, yield 6.76 g, 95%.

Synthesis of Compound 1-4: Horner-Wadsworth-Emmons procedure. The prodcuct was obtained from the evaporated organic phase and recrystallized from a EtOH/EtOAc mixture left. Yield 0.22 g (51 %), white powder. ^{1}H NMR (400 MHz, $CDCl_3$, ppm) δ: 8.05 (s, 1H), 7.09 (s, 1H), 7.60 (m, 4H), 7.43 (t, *J* = 7.2, 3.2 Hz, 4H), 7.39 (m, 2H), 7.36 (t, J = 4.0, 2.0 Hz, 2H), 7.29 (d, *J* = 7.5 Hz, 1H), 7.12 (d, *J* = 3.5 Hz, 1H).

Synthesis of Compound 2-1: 2-phenylacetonitrile (2.34 g, 20.0 mmol) were added to substituted 4-methylbenzaldehyde (3.00 g, 25.0 mmol) in ethanol (200 mL), after which the mixture was stirred at room temperature for 15 min. To this solution, sodium ethoxide (7.00 g, 100 mmol) in the same solvent (100 mL) was added dropwise with constant stirring, and the reaction mixture was vigorously stirred for 48 h to complete the reaction, which was monitored by TLC. After removal of the solid materials and solvent, crude products were purified by silica gel column chromatography (eluent: mixtures of dichloromethane and n-hexane from 7:3 gradient. ^{1}H NMR (400 MHz, $CDCl_3$, ppm) δ: 7.65 (d, *J* = 6.8 Hz, 2H), 7.46 (t, *J* = 7.5 Hz, 5H), 7.23 (d, *J* = 6.8 Hz, 2H), 7.02 (d, *J* =1.5 Hz, 1H), 2.41 (s, 3H).

Synthesis of Compound 2-2: The synthesis method is similar to compound 1-2, except that the equivalent of NBS is halved.

Synthesis of Compound 2-3: The synthesis method is similar to compound 1-3, except that the equivalent of triethylphosphite is halved.

Synthesis of Compound 2-4: Horner-Wadsworth-Emmons procedure. The prodcuct was obtained from the evaporated organic phase and recrystallized from a

EtOH/EtOAc mixture left. Yield 0.22 g (51 %), white powder. ^{1}H NMR (400 MHz, $CDCl_3$, ppm) δ: 8.04 (s, 1H), 7.98 (d, *J* = 8.0 Hz，2H), 7.78 (d, *J* = 6.0 Hz, 4H), 7.60 (s, 4H), 7.53 (m, *J* = 7.2 Hz, 2H), 7.46 (m, *J* =7.2 Hz, 1H), 7.39 (d, *J* = 3.6 Hz, 2H).

Synthesis of Compound 3-1: p-Tolunitrile (25.0 mL, 209 mmol) was added to 1,2-dicloroethane (400 mL) in a round-bottom flask with stirring. NBS (18.8 g, 105 mmol), and benzoyl peroxide (2.55 g, 10.5 mmol) were added, and the mixture was refluxed until the orange color disappeared (1.5 h). NBS (18.8 g, 105 mmol), and benzoyl peroxide (2.55 g, 10.5 mmol) were added, and the mixture was refluxed again for 1.5 h. The reaction mixture was allowed to stand overnight. The succinimide precipitate was removed by filtration. The filtrate was washed successively with water (200 mL), sat. aq. $NaHCO_3$ (200 mL), and brine (200 mL). The organic solution was dried over $MgSO_4$, and the solvent was removed in vacuo. The crude product was dissolved in toluene (100 mL). Trimethyl phosphite (60.0 mL, 508 mmol) was added, and the mixture was refluxed overnight. The solvent was removed in vacuo, and the crude product was purified by column chromatography (silica gel, 4:1 CH_2Cl_2:acetone) and then by recrystallization (1:1 ethyl acetate:hexanes) to give the title compound as an off-white crystalline solid (16.7 g, 35% over 2 steps). ^{1} H NMR (400 MHz, $CDCl_3$) δ: 3.17 (d, *J* = 2.0 Hz, 2H), 3.66 (d, *J* = 7.5 Hz, 6H), 7.37 (dd, *J* = 8.4, 2.0 Hz, 2H), 7.58 (d, *J* = 8.0 Hz, 2H).

Synthesis of Compound 3-2: Horner-Wadsworth-Emmons procedure. The product was obtained from the evaporated organic phase and recrystallized from a EtOH/EtOAc mixture left. Yield 0.22 g (51 %), white powder. ^{1} H NMR (400 MHz,

CD_2Cl_2) δ: 7.11 (d, *J* = 8.0 Hz, 1H), 7.18 (d, *J* = 7.5 Hz, 1H), 7.42 (d, *J* = 8.8 Hz, 2H), 7.52 (d, *J* = 8.8 Hz, 2H), 7.59 (d, *J* = 8.4 Hz, 2H), 7.65 (d, *J* = 8.4 Hz, 2H).

Synthesis of Compound 3-3: Compound 3-2 (448 mg, 1.80 mmol) was dissolved in DCM (10 mL) and cooled to 0 °C. DIBAL-H (1.0M in hexanes, 1.9 mL, 1.9 mmol) was added dropwise. After workup, the solvent was removed in vacuo to give the title compound as a white solid (423 mg, 93%). ^{1}H NMR (400 MHz, CD_2Cl_2) δ: 7.17 (1H, d, *J* = 8.4 Hz, 1H), 7.24 (d, *J* =8.0 Hz, 1H), 7.45 (d, *J* = 8.4 Hz, 2H), 7.53 (d, *J* = 8.4 Hz, 2H), 7.68 (d, *J* = 8.4 Hz, 2H), 7.87 (d, J = 8.4 Hz, 2H), 9.99 (s, 1H).

Synthesis of Compound 3-4: Horner-Wadsworth-Emmons procedure. The product was obtained from the evaporated organic phase and recrystallized from a EtOH/EtOAc mixture left. Yield 0.22 g (51 %), white powder. Solubility of the compound in standard deuterated solvents was insufficient to obtain satisfactory ^{1}H and ^{13}C NMR spectra.

General Procedure for Synthesis of SBz-Based Emitters. Under nitrogen atmosphere, Bromine-containing precursor compounds (1.0 equiv), diphenylamine (2.3 equiv), $Pd(OAc)_2$ (0.03 equiv), tri-tert-butylphosphine (0.09 equiv) and *t*-BuOK (6.0 equiv) were added to a Schlenk tube containing dry toluene (7 mL/mmol). The resulting mixture was stirred at 110 °C for 18 h. After cooling to room temperature, the mixture was extracted into CH_2Cl_2 and dried with anhydrous Na_2SO_4. After evaporated to dryness, the residue was purified by column chromatography over silica gel using proper eluent.

SBz-1. CH_2Cl_2:Petroleum ether = 1:2 (v/v); Yield: 86%. ^{1}H NMR (600 MHz, DMSO-

d_6) δ 8.39 (s, 1H), 7.67 (s, 1H), 7.61 (dd, J = 8.0, 1.5 Hz, 2H), 7.41 (t, J = 7.6 Hz, 3H), 7.37 (s, 1H), 7.35 – 7.27 (m, 8H), 7.26 – 7.21 (m, 3H), 7.07 – 6.97 (m, 7H). ^{13}C NMR (151 MHz, DMSO) δ 147.61, 146.14, 139.07, 135.90, 135.25, 133.64, 132.80, 131.56, 130.66, 128.93, 128.22, 128.14, 128.04, 127.52, 126.31, 125.73, 122.45, 122.12, 121.58, 117.15, 106.71; FAB-MS (m/z): 475 $[M]^+$; Anal. Calcd for $C_{35}H_{26}N_2$: C, 88.58; H, 5.25; N, 5.90; found: C, 88.61; H, 5.15; N, 5.85.

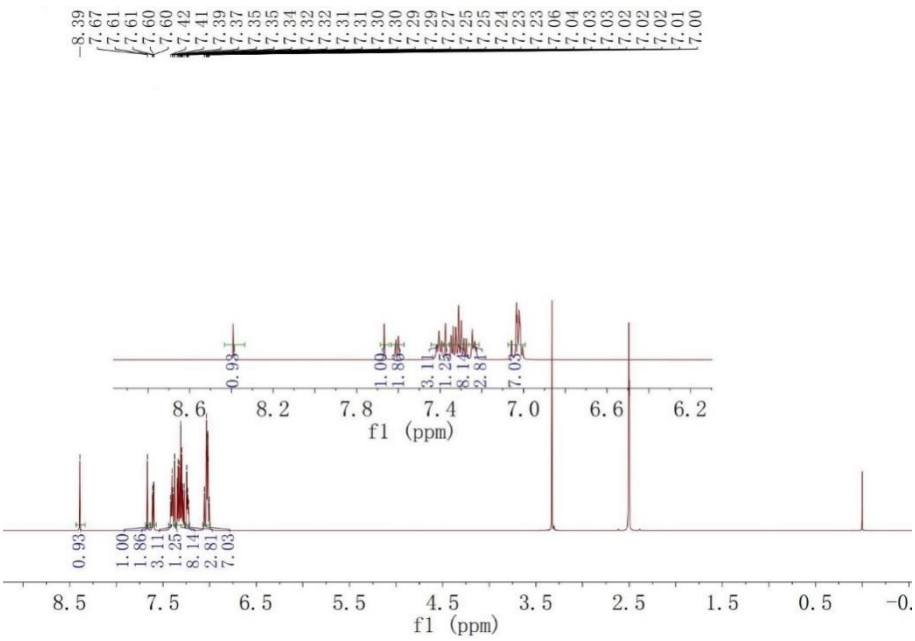

Figure S1 ^{1}H NMR spectrum of SBz-1 in $CDCl_3$.

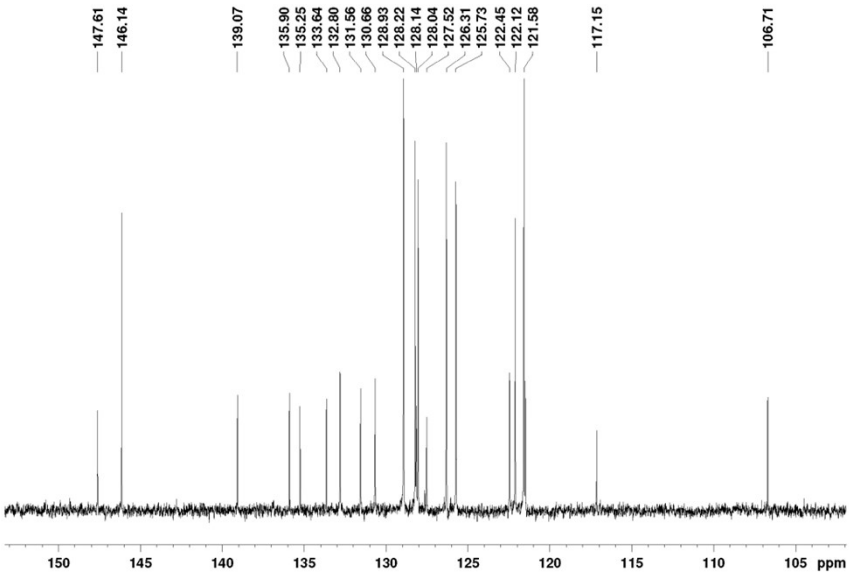

Figure S2 ^{13}C NMR spectrum of SBz-1 in $CDCl_3$.

SBz-2. CH_2Cl_2:Petroleum ether = 1:2 (v/v); Yield: 78%. ^1H NMR (600 MHz, $CDCl_3$) δ 7.90 (d, *J* = 8.2 Hz, 2H), 7.69 (d, *J* = 7.5 Hz, 2H), 7.58 (d, *J* = 8.2 Hz, 2H), 7.51 (s, 1H), 7.45 (t, *J* = 7.6 Hz, 2H), 7.41 (t, *J* = 7.6 Hz, 3H), 7.28 (t, *J* = 7.9 Hz, 4H), 7.19 – 7.09 (m, 5H), 7.09 – 6.98 (m, 5H). ^{13}C NMR (151 MHz, $CDCl_3$) δ 147.87, 147.39, 141.70, 140.03, 134.68, 132.42, 130.77, 130.17, 129.81, 129.33, 129.05, 127.65, 126.66, 125.93, 125.77, 124.69, 123.26, 123.19, 118.29, 110.45; FAB-MS (m/z): 475 $[M]^+$; Anal. Calcd for $C_{35}H_{26}N_2$: C, 88.58; H, 5.25; N, 5.90; found: C, 88.60; H, 5.09; N, 5.86.

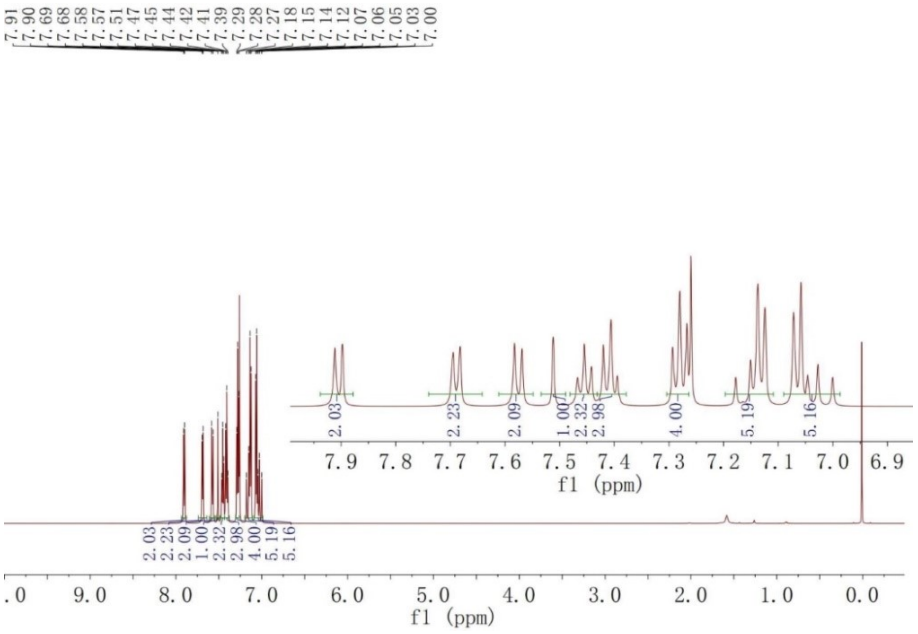

Figure S3 ^1H NMR spectrum of SBz-2 in $CDCl_3$.

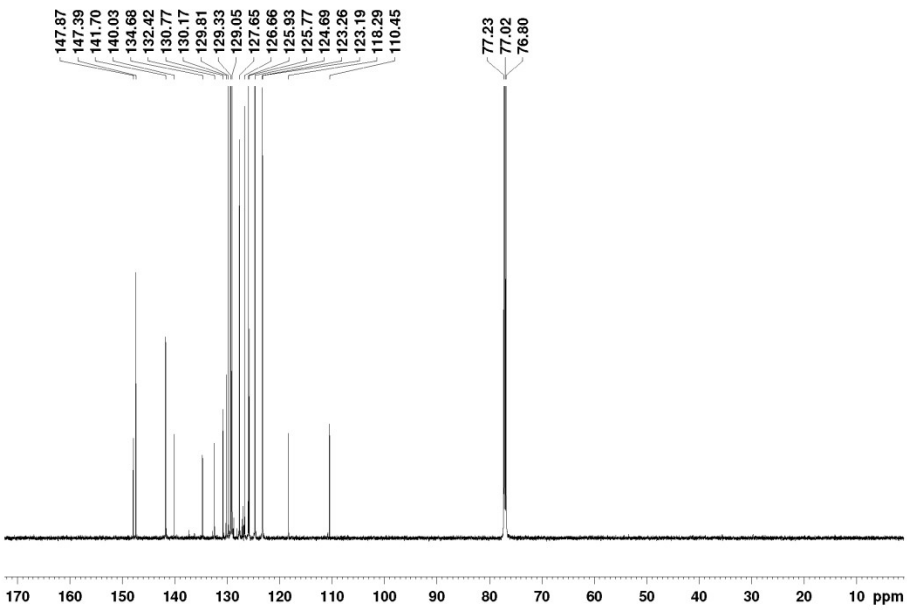

Figure S4 ^{13}C NMR spectrum of SBz-2 in $CDCl_3$.

SBz-3. CH_2Cl_2:Petroleum ether = 1:2 (v/v); Yield: 53%. ^1H NMR (600 MHz, Chloroform-*d*) δ 7.45 (d, *J* = 8.5 Hz, 2H), 7.35 (dd, *J* = 13.5, 8.6 Hz, 4H), 7.29 – 7.22 (m, 6H), 7.14 – 7.08 (m, 4H), 7.06 – 7.01 (m, 6H), 6.91 (d, *J* = 16.3 Hz, 2H). ^{13}C NMR (151 MHz, $CDCl_3$) δ 147.61, 147.44, 136.58, 131.72, 130.96, 129.30, 128.88, 127.74, 127.40, 125.61, 124.58, 123.38, 123.14, 120.85; FAB-MS (m/z): 475 $[M]^+$; Anal. Calcd for $C_{35}H_{26}N_2$: C, 88.58; H, 5.25; N, 5.90; found: C, 88.62; H, 5.10; N, 5.84.

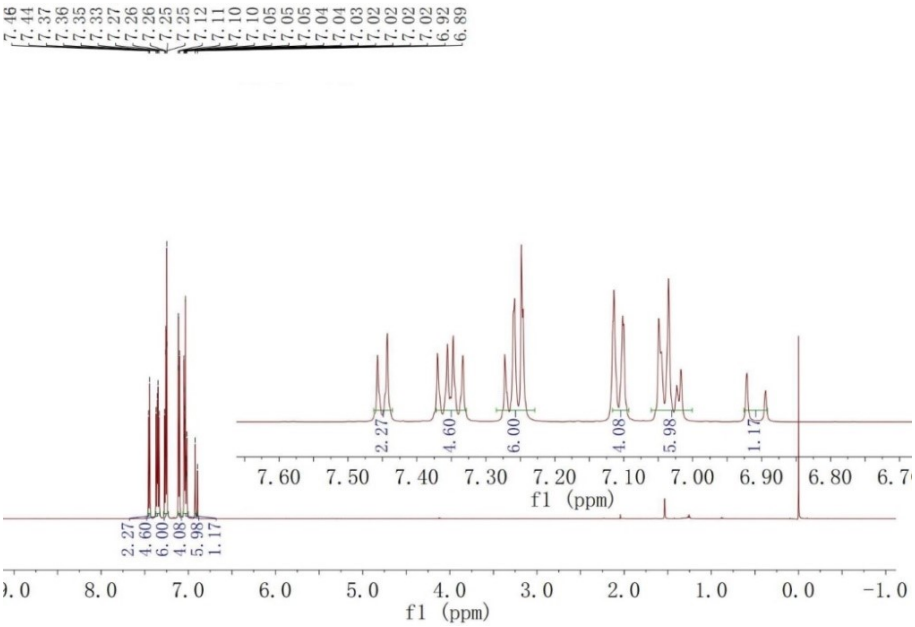

Figure S5 ^{1}H NMR spectrum of SBz-3 in $CDCl_3$.

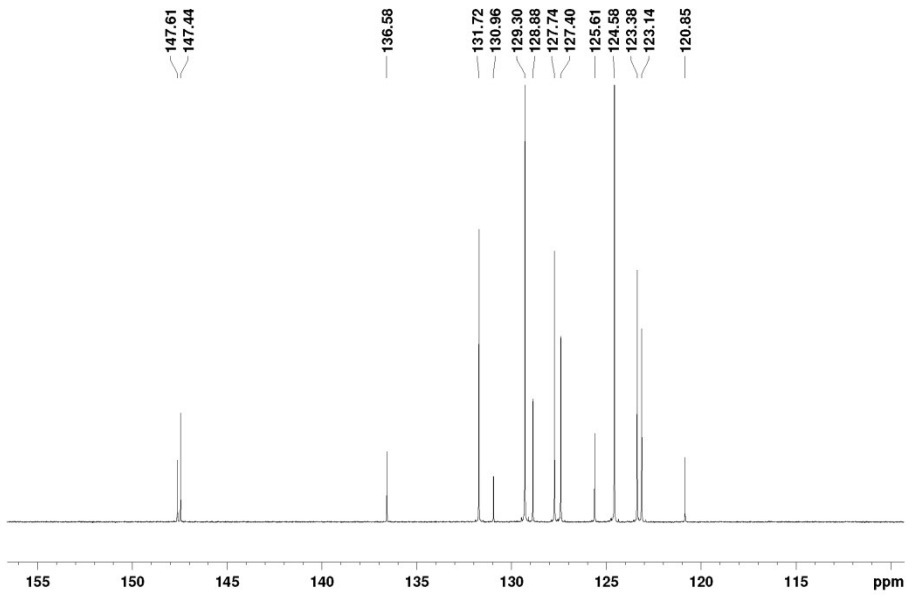

Figure S6 ^{13}C NMR spectrum of SBz-3 in $CDCl_3$.

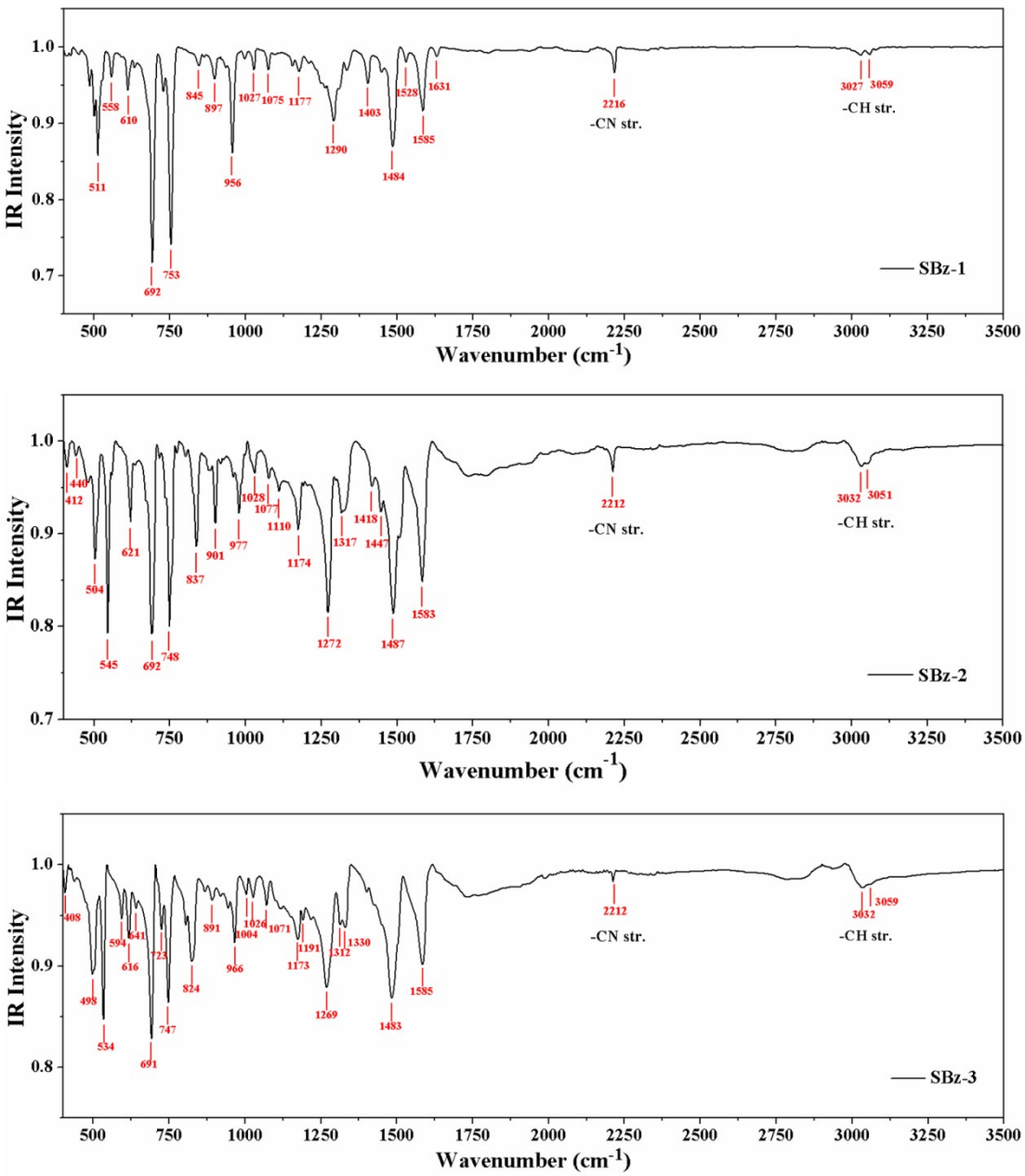

Figure S7 FTIR (KBr, cm^{-1}) spectra of the SBz-1, SBz-2 and SBz-3.

Table S1 FTIR selected peaks assignment for the SBz-1, SBz-2 and SBz-3.

Functional groups	-C-H (str.)	-CN (str.)	C=C (str.)	C-N (str.)
SBz-1	3027, 3059	2216	1585, 1528, 1484, 1403	1290
SBz-2	3032, 3051	2212	1583, 1487, 1447, 1418	1272
SBz-3	3032, 3059	2212	1585, 1483	1269

3. The solvatochromic Lippert-Mataga model

The Lippert-Mataga equation, that describes the interactions between the solvent and the dipole moment of solute were used to estimate the dipole moments of S_1 state:

$$hc(\nu_a - \nu_f) = hc(\nu_a^0 - \nu_f^0) - \frac{2(\mu_e - \mu_g)^2}{a_0^3} f(\varepsilon,n)$$

Take differential on both sides of the above equation, we got

$$\mu_e = \mu_g + \left\{\frac{hca_0^3}{2} \cdot \left[\frac{d(\nu_a - \nu_f)}{df(\varepsilon,n)}\right]\right\}^{1/2}$$

where h is the Plank constant, c is the light speed in vacuum, $f(\varepsilon,n)$ is the orientational polarizability of solvents, $\nu_a^0 - \nu_f^0$ is the Stokes shifts when f is zero, μ_e and μ_g are dipole moments of excited-state and ground-state, respectively; a_0 is the solvent Onsager cavity radius, derived from the Avogadro number (*N*), molecular weight (*M*), and density (d=1.0 g/cm^3); ε is the solvent dielectric constant and n is the solvent refractive index; μ_g of SBz-1, SBz-2, and SBz-3 could be estimated from a long-range-correction density-functional-theory (DFT) calculation at the level of CAM-B3LYP/6-31g(d,p) from Gaussian 09 package, which gave μ_g of 5.1 D, 4.2D, and 5.7 D, respectively. $f(\varepsilon,n)$ and a_0 can be calculated as follows:

$$f(\varepsilon,n) = \frac{\varepsilon - 1}{2\varepsilon + 1} - \frac{n^2 - 1}{2n^2 + 1}, \quad a_0 = \left(\frac{3M}{4N\pi d}\right)^{1/3}$$

The detailed data are listed in Table S1. For SBz-1, the μ_e was estimated to be 14.3 D and 15.4 D in low-polarity solvents (slope value of ≈ 8367, R= 0.71) and in high-polarity solvents (slope value of ≈ 10592, R= 0.93) respectively. For SBz-2, the μ_e was estimated to be 14 D and 18D in low-polarity solvents (slope value of ≈ 9307, R= 0.83) and in high-polarity solvents (slope value of ≈ 19941, R= 0.90) respectively.

While for SBz-3 the μ_e was estimated to be 12 D and 16 D in low-polarity solvents (slope value of ≈ 4838, R= 0.80 and in high-polarity solvents (slope value of ≈ 10650, R= 0.88) respectively.

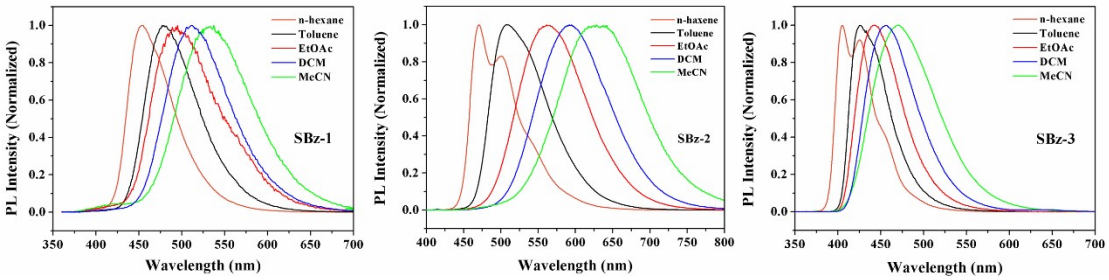

Figure S8 The PL spectra of SBz-1, SBz-2 and SBz-3 compounds in various solvents.

Table S2 The data about absorption and emission peak positions of SBz-1, SBz-2 and SBz-3 in various solvents.

Solvents	ε	n	$f(\varepsilon,n)$	SBz-1			SBz-2			SBz-3		
				λ_a (nm)	λ_f (nm)	ν_a-ν_f (cm^{-1})	λ_a (nm)	λ_f (nm)	ν_a-ν_f (cm^{-1})	λ_a (nm)	λ_f (nm)	ν_a-ν_f (cm^{-1})
Hexane	1.9	1.375	0.0012	345	460	7246	417	486	3405	374	415	2642
Toluene	2.38	1.494	0.014	346	482	8155	419	507	4142	375	425	3137
Triethylamine	2.42	1.401	0.048	344	464	7518	416	495	3836	374	418	2815
Butyl ether	3.08	1.399	0.096	346	475	7849	416	504	4197	374	428	3374
Isopropyl ether	3.88	1.368	0.145	344	489	8620	416	533	5277	374	429	3428
Ethyl ether	4.34	1.352	0.167	345	495	8784	418	531	5091	375	435	3678
Ethyl acetate	6.02	1.372	0.200	345	511	9416	417	561	6156	375	443	4093
Tetrahydrofuran	7.58	1.407	0.210	345	512	9454	419	572	6384	376	447	4224
dichloromethane	8.93	1.424	0.217	344	513	9577	418	592	7032	376	457	4714
Acetone	20.7	1.359	0.284	346	527	9926	422	627	7748	376	459	4809
Acetonitrile	37.5	1.344	0.305	346	540	10383	421	628	7829	376	469	5274

4. Photophysical properties

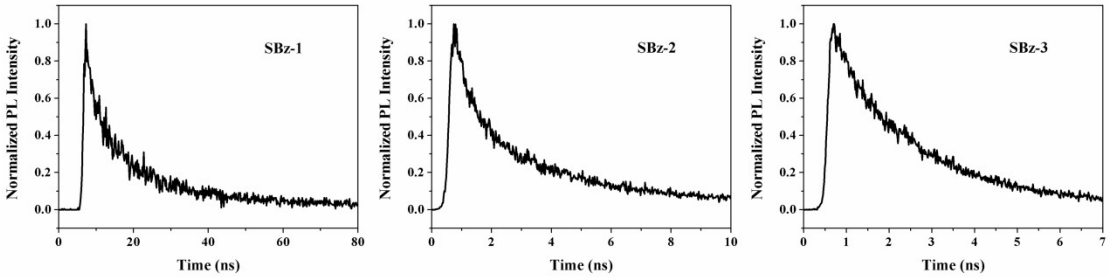

Figure S9 Lifetime measurement of SBz-1, SBz-2 and SBz-3 in doped solid-state films (6 wt% in CBP host).

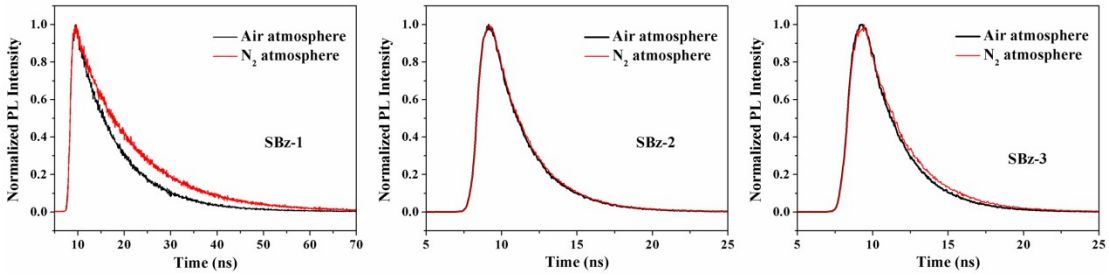

Figure S10 Lifetime measurement of SBz-1, SBz-2 and SBz-3 in THF solution in air and N_2 atmospheres.

Table S3 Lifetime parameters of SBz-1, SBz-2 and SBz-3 in THF solution in air and N_2 atmospheres.

Compounds	Air	N_2
SBz-1	9.55 ns	12.48 ns
SBz-2	2.47 ns	2.52 ns
SBz-3	2.44 ns	2.74 ns

It is noticeable that SBz-1, SBz-2 and SBz-3 do not possess delayed lifetime component, indicating that the three molecules are not TADF materials.

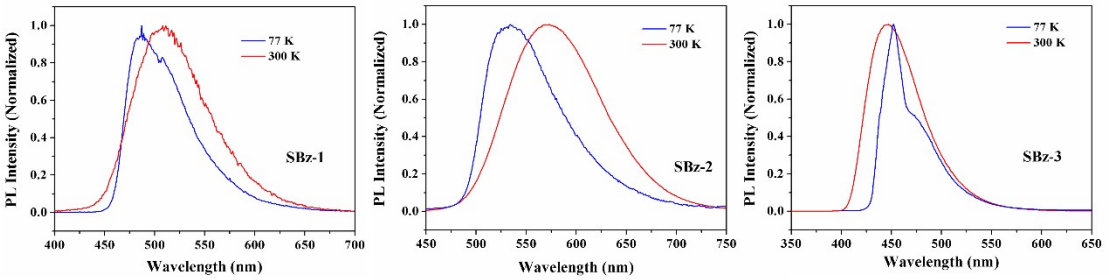

Figure S11 PL spectra of SBz-1, SBz-2 and SBz-3 in THF at 77 K and at 300 K.

5. Electroluminescence properties

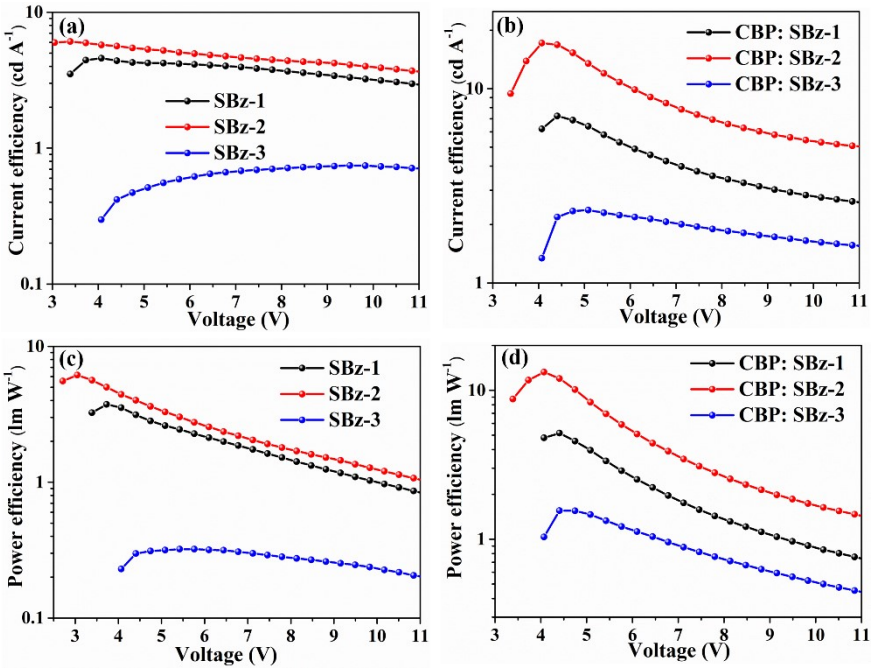

Figure S12 Current efficiency and power efficiency curve of these non-doped and doped devices based on SBz-1, SBz-2, and SBz-3.

6. Thermal properties

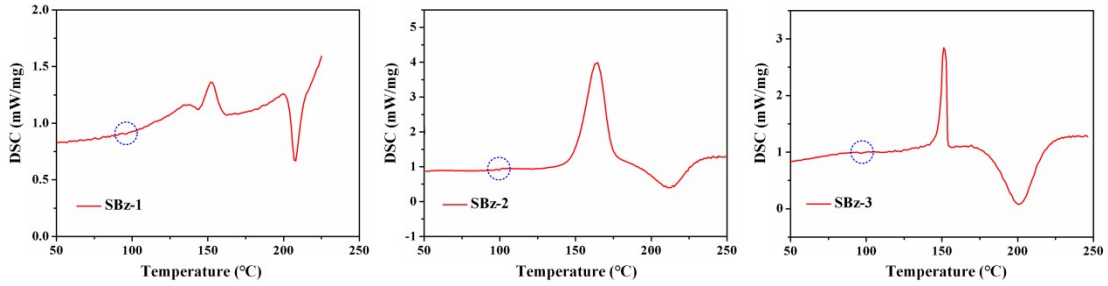

Figure S13 DSC curves of SBz-1, SBz-2 and SBz-3, at heating rate of 10 °C/min under nitrogen flushing.

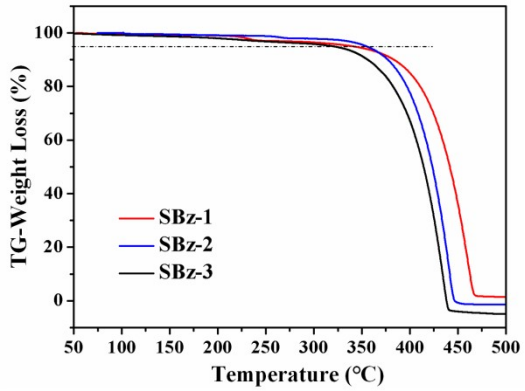

Figure S14 TGA curves of SBz-1, SBz-2 and SBz-3.

Table S4 Summary of the thermal properties.

Thermal Parameters (°C)	T_g	T_c	T_m	T_d
SBz-1	97.1	152.0	207.4	342.6
SBz-2	99.3	160.3	215.8	355.3
SBz-3	95.7	150.8	200.9	322.2

The thermal behaviors of SBz-1, SBz-2 and SBz-3 were investigated by means of Differential Scanning Calorimetric (DSC, Figure S13) and the thermogravimetric (TG) analyses (50-500 °C, Figure S14) at standard heating rate of 10 °C/min under nitrogen flushing. The thermal data is summarized in Table S4. In the scans shown in Figure S13, the three samples were heated to 250 °C. The SBz-1, SBz-2 and SBz-3 show the glass transition temperature (T_g) in the heating procedure at 97.1 °C, 99.3 °C and 95.7 °C. The crystallization peak (T_c) for SBz-1, SBz-2 and SBz-3 are at 152.0 °C, 160.3 °C and 150.8 °C. The SBz-1, SBz-2 and SBz-3 exhibit the melting temperature (T_m)

at 207.4 °C, 215.8 °C and 200.9 °C. The $\boldsymbol{T_d}$ for 5% mass loss (Figure S14) observed at 342.6 °C, 355.3 °C and 322.2 °C for SBz-1, SBz-2 and SBz-3 respectively.

7. Electrochemical properties

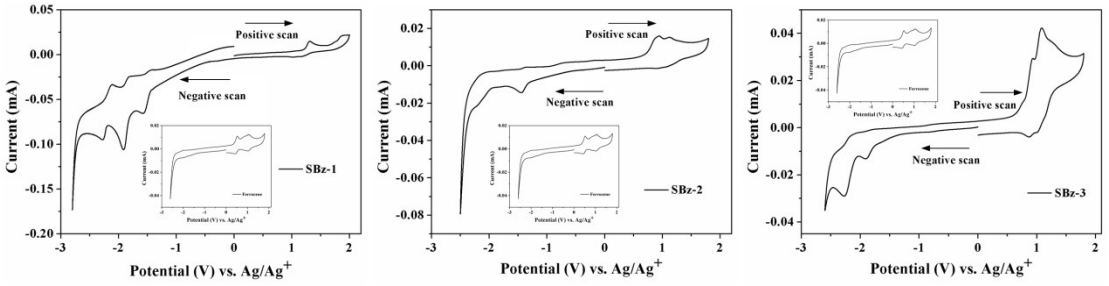

Figure S15 Cyclic Voltammograms (CV) of SBz-1, SBz-2 and SBz-3. Working electrode: glassy-carbon disk; counter electrode: Pt wire; reference electrode: Ag/Ag+. Scan rate: 50 mV/s. Electrolyte: 0.1 mol/L, TBAPF6 in MeCN.

Table S5 Electrochemical results from cyclic voltammetry of SBz-1, SBz-2 and SBz-3.

Compounds	E_{ox} (V)/HOMO (eV)	E_{red} (V)/LUMO (eV)	E_g (eV)
SBz-1	1.22/-5.93	-1.45/-3.26	2.67
SBz-2	0.62/-5.33	-1.96/-2.75	2.58
SBz-3	0.70/-5.41	-2.09/-2.62	2.79

The cyclic voltammograms (CVs) of SBz-1, SBz-2 and SBz-3 in THF solutions are shown in Figure S15, and the electrochemical properties are summarized in the Table S5. All the CVs show oxidation peak with the onset oxidation (positive scan) potentials E_{ox} at 1.22 V, 0.62 V and 0.70 V (vs. Ag/Ag^+), respectively. The SBz-1, SBz-2 and SBz-3 show the onset-reduction potentials (negative-scan) E_{red} at -1.45 eV, -1.96 eV and -2.09 eV. The E_{HOMO} and E_{LUMO} levels were estimated from the onset-oxidation and reduction potentials respectively by comparison to that of ferrocene according to the following equations: E_{HOMO}=-(E_{ox} vs. Ag/Ag^+ - $E_{1/2}$ vs. Ag/Ag^+ + 4.8) eV; E_{LUMO}=-(E_{red} vs. Ag/Ag^+ - $E_{1/2}$ vs. Ag/Ag^+ + 4.8) eV. Where the E_{ox} vs. Ag/Ag^+ and E_{red} vs. Ag/Ag^+ are the oxidation and reduction onset potentials relative to the Ag/Ag^+ electrode, respectively. The $E_{1/2}$ vs. Ag/Ag^+ is the half wave potentials ($E_{1/2}$=(E_{pa}+E_{pc})/2; 0.09 V) of Fc/Fc+. The calculation gives HOMO energy level,

E_{HOMO} for the SBz-1=-5.93 eV, SBz-2=-5.33 eV, and SBz-3=-5.41 eV. Similarly the E_{LUMO} levels calculated from the onset-reduction potentials are: E_{LUMO} for the SBz-1=-3.26 eV, SBz-2=-2.75 eV, and SBz-3=-2.62 eV. The electrochemical band gaps E_g for the SBz-1, SBz-2 and SBz-3 are 2.67 eV, 2.58 eV and 2.79 eV respectively.

8. Theoretical calculation: Natural transition orbit (NTO)

Compound	Singlet	Hole		Particle	Transition Character
SBz-1	$S_0 \rightarrow S_1$		98.54%		CT
	$S_0 \rightarrow S_2$		95.11%		LE
	$S_0 \rightarrow S_3$		90.29%		HLCT
	$S_0 \rightarrow S_4$		68.34%		HLCT
	$S_0 \rightarrow S_5$		49.66%		LE
	$S_0 \rightarrow S_6$		57.76%		LE
	$S_0 \rightarrow S_7$		94.51%		LE
	$S_0 \rightarrow S_8$		95.66%		LE
	$S_0 \rightarrow S_9$		82.59%		LE
	$S_0 \rightarrow S_{10}$		91.53%		LE

Compound	Triplet	Hole		Particle	Transition Character
SBz-1	$S_0 \rightarrow T_1$		88.76%		LE
	$S_0 \rightarrow T_2$		66.49%		LE
	$S_0 \rightarrow T_3$		85.28%		HLCT
	$S_0 \rightarrow T_4$		90.69%		LE
	$S_0 \rightarrow T_5$		79.31%		LE
	$S_0 \rightarrow T_6$		64.23%		LE
	$S_0 \rightarrow T_7$		69.17%		LE
	$S_0 \rightarrow T_8$		57.98%		LE
	$S_0 \rightarrow T_9$		74.81%		LE
	$S_0 \rightarrow T_{10}$		63.24%		LE

Figure S16 NTOs of the first ten singlet and ten triplet excited-states for SBz-1.

Compound	Singlet	Hole		Particle	Transition Character
SBz-2	$S_0 \rightarrow S_1$		99.51%		HLCT
	$S_0 \rightarrow S_2$		87.31%		HLCT
	$S_0 \rightarrow S_3$		88.48%		HLCT
	$S_0 \rightarrow S_4$		96.11%		LE
	$S_0 \rightarrow S_5$		98.94%		LE
	$S_0 \rightarrow S_6$		69.59%		HLCT
	$S_0 \rightarrow S_7$		62.70%		LE
	$S_0 \rightarrow S_8$		68.75%		LE
	$S_0 \rightarrow S_9$		63.85%		LE
	$S_0 \rightarrow S_{10}$		43.26%		LE

Compound	Triplet	Hole		Particle	Transition Character
SBz-2	$S_0 \rightarrow T_1$		91.28%		LE
	$S_0 \rightarrow T_2$		60.98%		LE
	$S_0 \rightarrow T_3$		73.41%		CT
	$S_0 \rightarrow T_4$		48.68%		HLCT
	$S_0 \rightarrow T_5$		83.67%		LE
	$S_0 \rightarrow T_6$		95.22%		LE
	$S_0 \rightarrow T_7$		48.54%		LE
	$S_0 \rightarrow T_8$		49.62%		HLCT
	$S_0 \rightarrow T_9$		84.62%		LE
	$S_0 \rightarrow T_{10}$		74.69%		LE

Figure S17 NTOs of the first ten singlet and ten triplet excited-states for SBz-2.

Compound	Singlet	Hole	Particle	Transition Character
SBz-3	$S_0 \rightarrow S_1$		99.40%	HLCT
	$S_0 \rightarrow S_2$		87.65%	HLCT
	$S_0 \rightarrow S_3$		84.61%	HLCT
	$S_0 \rightarrow S_4$		96.04%	LE
	$S_0 \rightarrow S_5$		98.96%	LE
	$S_0 \rightarrow S_6$		96.41%	CT
	$S_0 \rightarrow S_7$		52.88%	LE
	$S_0 \rightarrow S_8$		67.94%	LE
	$S_0 \rightarrow S_9$		68.41%	LE
	$S_0 \rightarrow S_{10}$		67.25%	HLCT

Compound	Triplet	Hole	Particle	Transition Character
SBz-3	$S_0 \rightarrow T_1$		92.72%	HLCT
	$S_0 \rightarrow T_2$		62.82%	LE
	$S_0 \rightarrow T_3$		65.89%	CT
	$S_0 \rightarrow T_4$		52.75%	LE
	$S_0 \rightarrow T_5$		83.56%	LE
	$S_0 \rightarrow T_6$		95.16%	LE
	$S_0 \rightarrow T_7$		38.12%	LE
	$S_0 \rightarrow T_8$		49.71%	LE
	$S_0 \rightarrow T_9$		49.71%	LE
	$S_0 \rightarrow T_{10}$		81.72%	LE

Figure S18 NTOs of the first ten singlet and ten triplet excited-states for SBz-3.

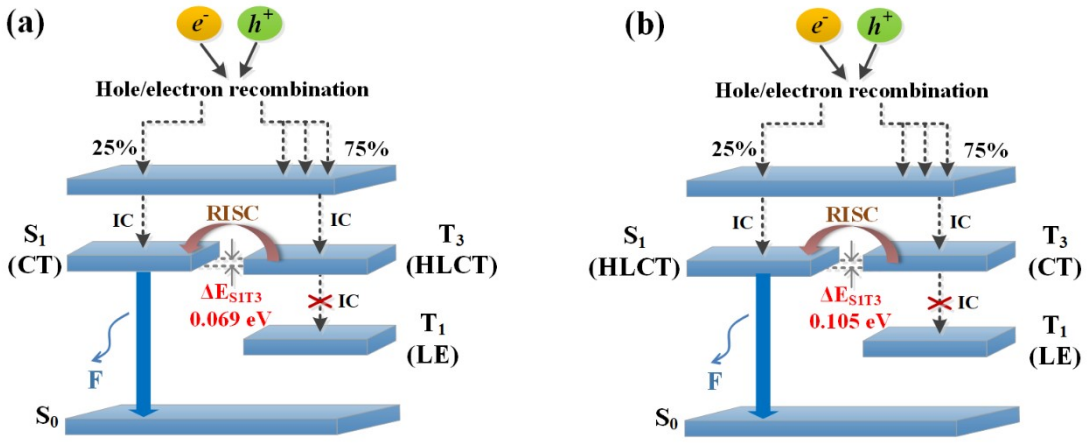

Figure S19 Probable ‘‘hot exciton’’ mechanism caused by the HLCT states based on compounds SBz-1 and SBz-2. S: singlet state; T: triplet state; LE: local excited state; HLCT: hybridized local and charge transfer excited state; ΔE_{ST}: singlet-triplet energy splitting; IC: internal conversion; RISC: reverse intersystem crossing.

9. Theoretical calculation: Elongation of vibrational modes

Under the adiabatic approximation, the electronic ground and excited state wave functions can be expressed as products of an electronic and nuclear part. Assuming a single vibronic coordinate for simplicity, the vibronic part of the total wave function contributes only a Frank-Condon overlap factors. The probability to emit through a transition from the lowest vibronic level $|0_e>$ of the first excited-state vibronic to the electronic ground state vibronic level $|n_g>$ with an electric field E at energy E_L is given by Fermi's golden rule [3]:

$$P\left(\left|0_e\right\rangle \rightarrow \left|n_g\right\rangle\right) = \frac{2\pi}{\hbar}\left|\vec{E}\cdot\vec{\mu}\right|^2 \left|\left\langle 0_e \middle| n_g \right\rangle\right|^2 \times \delta\left(E_L + E_{HOMO} - E_{LUMO} - n_g\hbar\omega\right)$$

where μ is the electronic transition dipole and the Franck-Condon factor can be defined as Poisson distribution:

$$\left|\left\langle 0_e \mid n_g \right\rangle\right|^2 = \frac{S^n}{n!}e^{-S}$$

In the Poisson distribution over the vibronic levels, S is Huang-Rhys factor which represents the vibronic coupling strength:

$$S_j = \frac{\omega(\Delta Q_j)^2}{2\hbar}$$

where ΔQ_j represents the displacement along the normal mode $(NM)_j$ between the equilibrium positions of the two electronic states.

Table S6 Selected normal vibrational modes (S>0.1) and relevant parameters of SBz-1, SBz-2 and SBz-3.

Selected vibrational frequencies ($\hbar\omega_j$), Huang-Rhys factors (S_j) and reorganization energies (λ_j) of compound SBz-11.

	$\hbar\omega_j$ (cm^{-1})	S_j	λ_j (cm^{-1})
Low-frequency Modes	32	0.636192	20.3
	54	2.036162	110.3
	64	0.2592	16.5
	77	2.5969205	199.6
	97	5.3138	513
	131	0.538722	70.5
	162	0.559682	90.8
	253	0.276768	70
	539	0.1070312	42.6
High-frequency Modes	1655	0.1326125	219.3
	1663	0.1664645	276.8
	1738	0.1915805	333.3

Selected vibrational frequencies ($\hbar\omega_j$), Huang-Rhys factors (S_j) and reorganization energies (λ_j) of compound SBz-2.

	$\hbar\omega_j$ (cm^{-1})	S_j	λ_j (cm^{-1})
Low-frequency Modes	32	0.209952	6.7
	40	0.182408	7.3
	54	0.122018	6.6
	118	0.619385	72.8
	133	0.376712	50.3
High-frequency Modes	1211	0.1058	128
	1219	0.135721	165.8
	1668	0.343621	573.4

Selected vibrational frequencies ($\hbar\omega_j$), Huang-Rhys factors (S_j) and reorganization energies (λ_j) of compound SBz-3.

	$\hbar\square_j$ (cm^{-1})	S_j	$\square_j$ (cm^{-1})
Low-frequency Modes	21	0.1806005	3.8
	76	0.155682	11.9
	105	0.445568	46.9
	112	0.51005	57.4
	1208	0.1185845	143.1
High-frequency Modes	1627	0.125	203.1
	1664	0.264992	440.5
	1666	0.1630205	271.3

References:

[1] Z. L. Cai and J. R. Reimers, *J. Phys. Chem. A*, 2000, **104**, 8389-8408.

[2] Dalton, a molecular electronic structure program, Release Dalton, 2013, see http://daltonprogram.org.

[3] I. Vragovic, R. Scholz, M. Schreiber, *Euro. Phys. Lett.* **2002**, *57*, 288-294.